Sensors & Actuators: B. Chemical 331 (2021) 129438

Contents lists available at ScienceDirect

Sensors and Actuators: B. Chemical

journal homepage: www.elsevier.com/locate/snb

Tunable construction of crystalline and shape-tailored Co_3O_4@TAPB-DMTP-COF composites for the enhancement of tert-butylhydroquinone electrocatalysis

Yuling Chen [a], Yao Xie [a], Xin Sun [a], Yang Wang [a,*], Yi Wang [b,*]

[a] School of Chemistry and Chemical Engineering, Yangzhou University, Yangzhou, 225002, China
[b] School of Biomedical Engineering, School of Ophthalmology & Optometry, Wenzhou Medical University, Wenzhou, 325027, China

ARTICLE INFO

Keywords:
Core-shell structure
Co_3O_4
TAPB-DMTP−COF
TBHQ

ABSTRACT

In this work, a monomer-mediated in situ growth strategy was developed for the controllable construction of core-shell Co_3O_4@TAPB-DMTP−COF composite (TAPB, 1,3,5-tris(4-aminophenyl)benzene; DMTP, 2,5-dimethoxyterephaldehyde; COF, covalent organic framework), which exhibits uniform size, high surface area, outstanding thermochemical stability, and ultrahigh effective surface area. The Co_3O_4@TAPB-DMTP−COF was further applied to develop an electrochemical sensor for the sensitive and selective determination of tert-butylhydroquinone (TBHQ). Mechanism investigations reveal that multistacked columnar channels given by TAPB-DMTP−COF shell can effectively facilitate the diffusion of TBHQ molecules to the active Co^{3+} sites. Under the optimal conditions, the current response exhibits two linear dynamic ranges, 0.05−1.0 and 1.0−400 μmol L^{-1}, and the detection limit was as low as 0.02 μmol L^{-1} (S/N = 3). Little to no interference effects from other co-existing ions allows the sensor to detect low-abundance TBHQ from complicated real samples. This study not only provides a strategy for crystalline and shape-tailored growth of COF shells, but also expands their further use in electrochemical sensor.

1. Introduction

Tert-butylhydroquinone (TBHQ) is one of frequently used synthetic phenolic antioxidants (SPAs) in edible oils due to its strong anti-lipid peroxidation activity, and high chemical stability [1,2]. Howbeit, health studies have indicated that high doses of TBHQ in foodstuffs may induce toxicological and mutagenic effects towards laboratorial animals [3,4]. Because of the potential risk of TBHQ, many countries (such as Brazil, the United States, and China) have created regulatory agencies that formulated the maximum permitted level in food of 200 mg kg^{-1} [5].

At present, high performance liquid chromatography (HPLC) equipped with different detection systems are the most conventional and popular analytical method for the accurate TBHQ determination in edible oils and foods [6,7]. While the universally proven technique of HPLC, the chromatographic method usually suffers from the deficiencies in sophisticated prior separation or sample clean up, costly and complicate instrument, entailing well-trained operators, and inapplicability for field use. Against such circumstances, electrochemical sensing is favored by researchers due to their fast response, relatively simple instrument, and ease of operation [8].

Covalent organic framework (COF) is an emerging class of porous crystalline materials, and constructs solely from light elements (H, C, B, N, O, etc.) linked by strong covalent bonds [9,10]. The high adaptability in the structural and functional designs, together with their inherent properties such as large surface areas, ordered channel structure, and outstanding thermochemical stability, have made COF excellent candidates in gas storage and separation [11,12], catalysis [13], drug delivery [14], and sensing [15]. Two-dimensional (2 D) COF is particularly interesting in electrochemical sensors because of its comprising eclipsed and ordered π-columnar structures [16,17]. The inherent eclipsed stacked structure in 2 D COF is ideally suitable for accommodating the guest molecules through the multi-stacked columnar channel. As one eminent representative, TAPB-DMTP−COF, which combines better chemical stability, higher crystallinity and porosity than other types of COF, has received significant attention in the chemical literatures [18,19]. However, further exploration of TAPB-DMTP−COF in the electrochemical field is still limited because the individual COF generally

* Corresponding authors.
E-mail addresses: wangyzu@126.com (Y. Wang), wangyi@wiucas.ac.cn (Y. Wang).

https://doi.org/10.1016/j.snb.2021.129438
Received 12 October 2020; Received in revised form 30 December 2020; Accepted 31 December 2020
Available online 5 January 2021

suffers from insignificant electrical conductivity [20]. Against such backdrop, controllable synthesis of 2 D COF or composite with electronic and catalytic traits is of considerable importance.

In the past years, integrating functional components predictably and deliberately to acquire core-shell-structured composite materials have attracted tremendous attention [21,22]. The composites are predetermined to have elegant combined properties of individual component. Cobalt oxide (Co_3O_4) is deemed as a promising catalytic material in the field of electrochemical sensor owing to its excellent electrocatalytic, low-priced, and chemically reactive properties [23,24].

In this work, a monomer-mediated in situ growth strategy was proposed for the controllable growth of COF shells on the Co_3O_4 dodecahedrons. Under the optimal conditions, the obtained Co_3O_4@TAPB-DMTP−COF based sensor exhibits excellent electrocatalytic properties towards TBHQ compared with other published sensors. The outstanding electronic and catalytic properties of Co_3O_4 core, accompanied with large surface area provided by TAPB-DMTP−COF shell guarantee the high sensitivity and selectivity towards TBHQ. Additionally, the established method was applied to detect TBHQ in different edible oils and satisfactory recoveries were received.

2. Experimental section

2.1. Synthesis of Co_3O_4 dodecahedrons

The preparation of Co_3O_4 dodecahedrons was carried out as follows [25]: 0.29 g $Co(NO_3)_3{\cdot}6H_2O$ was dissolved in 30 mL ethanol-water mixed solution (v/v, 1:1). Next, 0.2 g PVP was added into the solution and stirred for 10 min. Then, the light pink solution was transferred to a Teflon-lined autoclave and hydrothermally heated at 180 °C for 12 h. After cooling down to room temperature, the black precipitation was collected by centrifugation and washed with water and ethanol for three times. Finally, the Co_3O_4 particles were dried in a vacuum at 60 °C for 12 h.

2.2. Synthesis of amino functionalized Co_3O_4 dodecahedrons (Co_3O_4-NH_2) [26]

APTES (0.5 mL) was added to a suspension of Co_3O_4 (150 mg) in toluene (20 mL) under nitrogen atmosphere. The reaction was allowed to proceed for 2 h at 110 °C. After cooling down to room temperature, the product was washed with water for three times and dried in a vacuum for 12 h.

2.3. Synthesis of DMTP grated Co_3O_4 dodecahedrons (Co_3O_4-DMTP)

150 mg Co_3O_4-NH_2 particles were dispersed in 4.5 mL 1,4-dioxane-butanol-methanol (v/v/v, 4:4:1) cosolvent system, followed by adding 10 mg DMTP monomer and 2 mL HAc (3 mol · L^{-1}). After sonication for 5 min, the mixture was transferred to a Teflon-lined autoclave and hydrothermally heated at 120 °C for 1 h. After cooling down to room temperature, the Co_3O_4-DMTP particles were washed with 1,4-dioxane and THF twice before being dried in a vacuum.

2.4. Synthesis of Co_3O_4@TAPB-DMTP−COF core-shell composite

Typically, the obtained Co_3O_4-DMTP (20 mg) was dispersed in 4.5 mL cosolvent system. Then, the TAPB (0.030 mmol, 10.5 mg) and DMTP (0.045 mmol, 8.7 mg) monomer were added in the above cosolvent system and sonicated for 5 min. Afterwards, 0.67 mL HAc (9 mol · L^{-1}) was slowly dropped to the mixture. The vial was sealed and left undisturbed in an oven at 70 °C for 72 h. The resultant product was isolated by centrifugation and washed with 1,4-dioxane and THF twice, and finally dried at 60 °C for 12 h.

2.5. Preparation of the Co_3O_4@TAPB-DMTP−COF modified glassy carbon electrode (Co_3O_4@TAPB-DMTP−COF/GCE)

Before surface modification, the bare GCE (D = 3 mm) was polished to a mirror-like surface with 0.03 μm alumina/water slurry. Subsequently, the electrode was rinsed thoroughly with ethanol and dried with nitrogen blow. The detailed process of preparing modified electrode was: 1 mg Co_3O_4@TAPB-DMTP−COF core-shell composite was uniformly dispersed in 1 mL water. Then, 5 μL Co_3O_4@TAPB-DMTP−COF was dropped on the electrode surface. Two hours later, the solvent was dried in a desiccator and the modified electrode was finally prepared. The same procedure is capable to prepare other electrodes shown in this paper.

2.6. Sample preparation

Edible oil samples, including peanut oil, soybean oil, and colza oil were purchased from a local supermarket and pretreated for TBHQ analysis. In brief, 5 mL edible oil sample and 10 mL ethanol were added to a 50 mL centrifuge tube. And then, the mixture was agitated vigorously for 10 min using a vortex mixer and centrifuged at 8000 rpm for 5 min. The supernatant was collected and the residues were extracted twice. Afterwards, the obtained supernatant was evaporated in a vacuum at 60 °C and diluted with ethanol in a 50 mL volumetric flask. Before use, all solutions were kept in a refrigerator.

3. Results and discussion

3.1. Synthesis strategy and characterization of Co_3O_4@TAPB-DMTP−COF core-shell-structured composite

The general synthetic route for Co_3O_4@TAPB-DMTP−COF core-shell-structured composite is illustrated in Scheme 1. In order to improve the uniformity of COF shells, a monomer of DMTP was pre-grafted on the amino-functionalized Co_3O_4 (Co_3O_4-NH_2) via the Schiff base condensation reaction. Then, Co_3O_4-DMTP was acted as a heterogeneous nucleation site to support the in situ growth of TAPB-DMTP−COF. In a preliminary effort, we tried to directly grow TAPB-DMTP−COF on the Co_3O_4-NH_2 surface, but we observed that an incomplete incorporation towards Co_3O_4-NH_2 as well as the aggregation of amorphous 2D COF (Fig. S1). The results manifest that the monomer-mediated in situ growth strategy plays a pivotal role in constructing uniform crystalline COF shells.

The evolution of imine−COF involved an amorphous-to-crystalline transformation process [27]. In light of this, we explored the key factors which are favorable for the long-range molecular ordering in the 2D topological structure. When the reaction time was increased, the crystallization for TAPB-DMTP−COF shell was greatly improved (Fig. S2). This result implies that a time-dependent self−correction process in the TAPB-DMTP−COF shell makes for the formation of long periodic ordered structure. As the only catalyst for the synthesis of imine−COF, the concentration of acetic acid poses great influence on the TAPB-DMTP−COF crystallinity. As shown in Fig. S3, when 9 mol · L^{-1} acetic acid aqueous solution was utilized, the TAPB-DMTP−COF shell displayed the highest intense (100) peak at around 2.7°. In addition, TEM images shows that the morphology of TAPB-DMTP−COF shell varied with the concentration of acetic acid, which is basically conformation with the morphologies of pure TAPB-DMTP−COF prepared under the same conditions (Fig. S4). All above results show that the control of reaction time and concentration of acetic acid guarantee a crystalline and shape-tailored growth of TAPB-DMTP−COF shell in the composite.

The detailed crystallographic structure of the Co_3O_4@TAPB-DMTP−COF composite was displayed in Fig. 1B. As revealed in the XRD pattern of Co_3O_4 particles, the diffraction peaks centered at 19.0°, 31.2°, 36.8°, and 44.7° corresponded to (111), (220), (311), and (400)

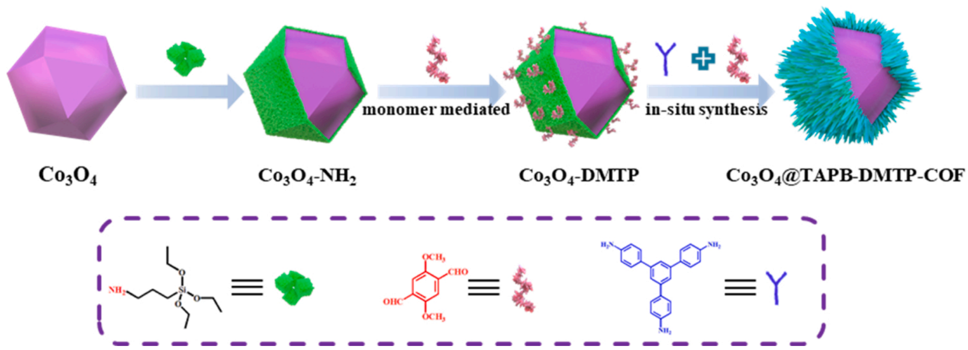

Scheme 1. Illustration of monomer-mediated in situ growth strategy for the synthesis of Co_3O_4@TAPB-DMTP−COF core-shell-structured composite.

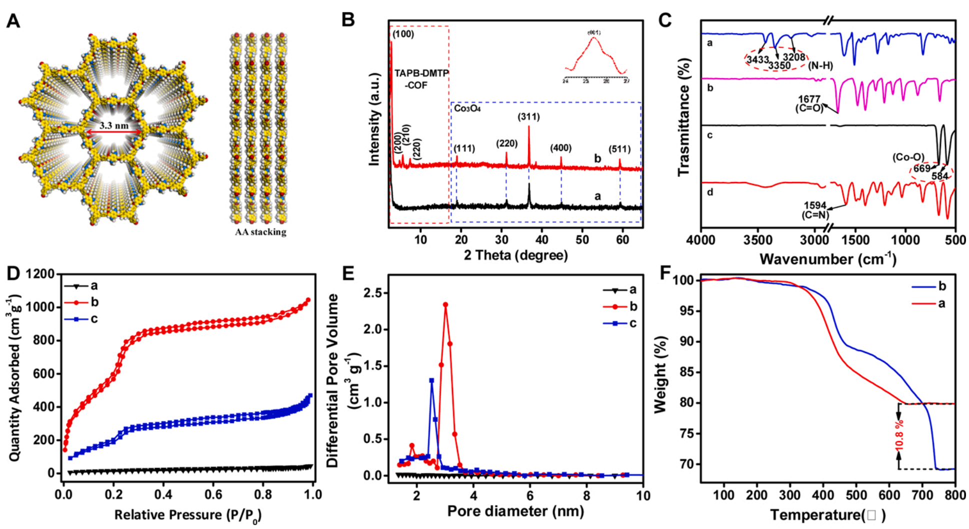

Fig. 1. The crystal structures of TAPB-DMTP−COF viewed through (001) (left) and (100) (right) reflection planes. (B) XRD patterns of Co_3O_4 (a), and Co_3O_4@TAPB-DMTP−COF (b). (C) FT-IR patterns of TAPB (a), DMTP (b), Co_3O_4 (c), and Co_3O_4@TAPB-DMTP−COF composite (d). (D)The nitrogen isotherms and (E) pore size distribution of Co_3O_4 (a), TAPB-DMTP−COF (b), and Co_3O_4@TAPB-DMTP−COF composite (c). (F) TGA plot of Co_3O_4 (a) and Co_3O_4@TAPB-DMTP−COF composite (b).

reflection planes, respectively. All these diffraction peaks can be well indexed with the typical spinel Co_3O_4 phase from the JCPDS NO 43-1003. Moreover, in addition to the Co_3O_4 peaks, the Co_3O_4@TAPB-DMTP−COF composite features a prominent intense peak at 2.7° assignable to (100) reflection plane, with the other diffraction peaks centered at 4.8°, 5.6°, 7.4°, and 25.4° corresponding to (200), (210), (220), and (001) reflection planes [18], indicating the presence of 2D eclipsed stacking TAPB-DMTP−COF in the composite. To shed light on the core-shell morphology of Co_3O_4@TAPB-DMTP−COF composite, TEM and energy dispersive X-ray spectroscopy (EDS) elemental mapping were conducted (Fig. 2). The uniform distribution of C atom along the Co in the core region unambiguously confirmed the formation of core-shell-structured Co_3O_4@TAPB-DMTP−COF.

The chemical structure of the samples was characterized by the Fourier-transform infrared (FT-IR) spectroscopy (Fig. 1C). In the IR spectrum of Co_3O_4, two intensive bands at 669 cm^{-1} and 584 cm^{-1} were associated with the metal-oxide stretching vibration of Co^{III}-O and Co^{II}-O, which originated from the tetrahedrally coordinated Co^{3+} and octahedrally coordinated Co^{2+} vibrations in the cubic spinel lattice of Co_3O_4, respectively [28]. In contrast with the Co_3O_4 and the monomers of TAPB and DMTP, the spectrum of Co_3O_4@TAPB-DMTP−COF revealed the emerging C═N stretch at 1594 cm^{-1}, along with the disappearance of the C═O vibration of DMTP (1677 cm^{-1}) and N—H vibrations of TAPB (3433, 3350, and 3208 cm^{-1}). The results further confirmed the successful formation of crystalline TAPB-DMTP−COF shell via the imine condensation reaction. Meanwhile, characterization of Co_3O_4-DMTP and Co_3O_4@TAPB-DMTP−COF composite by XPS also provided convincing evidence for the imine formation through amine and aldehyde groups. As displayed in Fig. 3B, Co_3O_4@TAPB-DMTP−COF

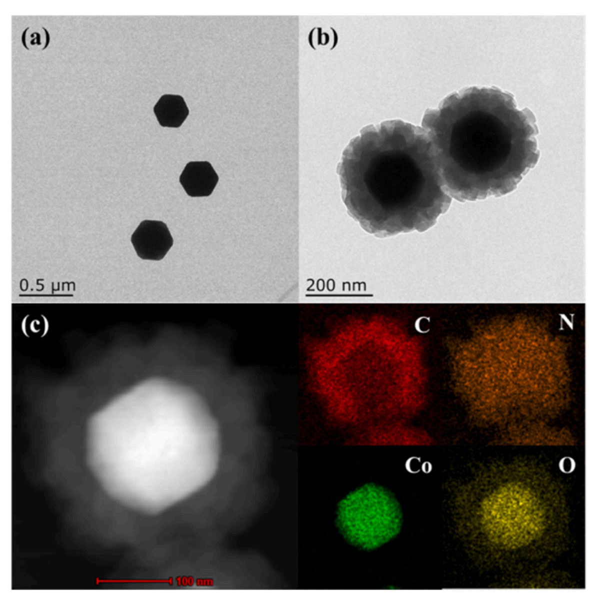

Fig. 2. TEM images of Co_3O_4 (a) and Co_3O_4@TAPB-DMTP−COF composite (b). EDS-TEM elemental mapping (c) of C, N, Co, O for Co_3O_4@TAPB-DMTP−COF composite.

composite exhibited a new strong peak at 398 eV, revealing the dramatically formation of -N=C- functional groups after TAPB-DMTP−COF coating.

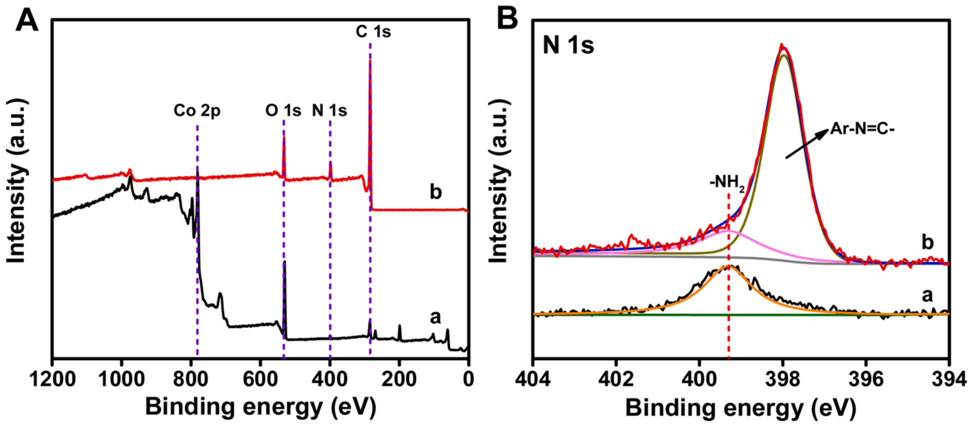

Fig. 3. (A) XPS survey spectra and (B) N 1s core-level XPS spectra of Co_3O_4-DMTP (a) and Co_3O_4@TAPB-DMTP−COF composite (b).

The permanent porosity of Co_3O_4@TAPB-DMTP−COF was determined by nitrogen adsorption-desorption isotherms at 77 K (Fig. 1D and E, Table S1). As shown in Fig. 1D, the isotherm curves of Co_3O_4@TAPB-DMTP−COF was observed with typical type IV characteristics according to the IUPAC classifications, indicating the presence of mesoporous structure. Distinctly, the prepared Co_3O_4@TAPB-DMTP−COF composite displayed an enlarged Brunauer-Emmett-Teller (BET) surface area to a value of 1234 $m^2 \cdot g^{-1}$ (*cf.* 56 $m^2 \cdot g^{-1}$ for Co_3O_4). By using the Barrett-Joyner-Halenda (BJH) model, only one type of pore width predominated at 2.5 nm was obtained in Co_3O_4@TAPB-DMTP−COF, which is in good agreement with the crystal structure of TAPB-DMTP−COF (Fig. 1A and E). The high external surface area and porosity of Co_3O_4@TAPB-DMTP−COF make it possible to be an excellent signal enhancer.

Thermogravimetric analysis (TGA) measurement was conducted to evaluate the mass ratios and thermal stability of the different components (Fig. 1F). The Co_3O_4@TAPB-DMTP−COF composite showed almost 31.9 wt% weight loss in the temperature range of 30–800 °C, which is 10.8 wt% over the bare Co_3O_4 particles, implying the high yield of TAPB-DMTP−COF shell on the surface of Co_3O_4. In addition, an unconspicuous weight-loss step of 0.94 % up to ca. 350 °C was found, demonstrating the excellent thermal stability of the Co_3O_4@TAPB-DMTP−COF composite.

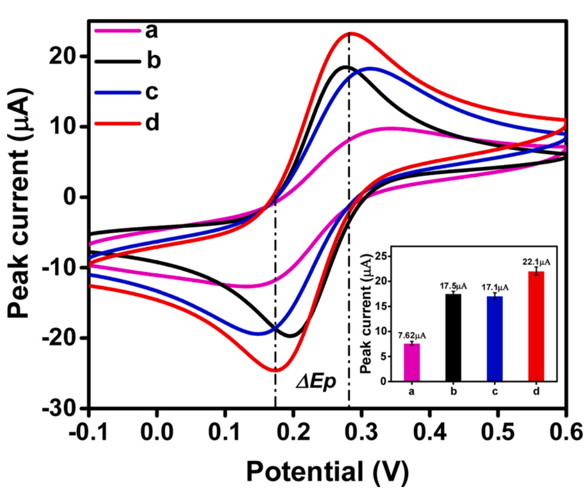

Fig. 4. CVs of 0.5 mmol · L^{-1} $[Fe(CN)_6]^{3-/4-}$ containing 0.1 mol · L^{-1} KCl at bare GCE (a), Co_3O_4/GCE (b), TAPB-DMTP−COF/GCE (c) and Co_3O_4@TAPB-DMTP−COF/GCE (d). Scan rate: 100 mV · s^{-1}.

3.2. Electrochemical behavior of core-shell Co_3O_4@TAPB-DMTP−COF composite

Cyclic voltammograms (CVs) can allow us to gain more direct insight into the electrical attributes of an electrode material. Fig. 4 shows the CV profiles of different electrodes in the ferricyanide redox probe ($[Fe(CN)_6]^{4-/3-}$) system. Compared with bare GCE, both a narrowed redox peak potential separation (ΔE_p) and enhanced peak current value can be observed after modifying with Co_3O_4 and Co_3O_4@TAPB-DMTP−COF. It is noteworthy that the ΔE_p value in a cyclic voltammogram is one of the important factors to estimate the electron charge transfer rate at the electrodel electrolyte interface. In a typical process, the ΔE_p value is inversely proportional to the charge transfer rate constant [29]. Here, the ΔE_p values were decreased in a sequence of TAPB-DMTP−COF/GCE (141 mV) > GCE (128 mV) > Co_3O_4@TAPB-DMTP−COF/GCE (97 mV) > Co_3O_4/GCE (70 mV). The above results indicated that the engineered of TAPB-DMTP−COF with Co_3O_4 can largely minimize the electron transfer barrier between the redox species and an electrode. Moreover, as seen in Fig. 4 inset, it can be found that the Co_3O_4@-TAPB-DMTP−COF/GCE displays the highest oxidation peak current, which is an indicative of superior electrocatalytic activity for electrochemical detection.

The effective surface areas of different electrocatalysts were also characterized by CVs at various scan rates (Fig. S5). For a reversible couple, the effective surface areas of different modified electrodes were calculated using following Randles-Sevcik equation [30]:

$$I_p = (2.69 \times 10^5) n^{3/2} D^{1/2} v^{1/2} AC$$

where n represents the numbers of electron transferred in the electrochemical process, D is the diffusion coefficient (in cm^2/s), v represents the scan rate (in V/s), C is the concentration of redox species (in mmol/L), A is the effective surface area (in cm^2). For ferricyanide redox probe, the electron number is 1 and the diffusion coefficient is 7.6×10^{-6} cm^2/s. After calculation, the obtained effective surface areas were as follows: 0.067, 0.098, 0.093, and 0.151 cm^2 for GCE, Co_3O_4/GCE, TAPB-DMTP-COF/GCE, and Co_3O_4@TAPB-DMTP−COF/GCE. Surprisingly, the effective surface area of Co_3O_4@TAPB-DMTP−COF/GCE was 2.3 times higher than the bare GCE. This markedly increase in effective surface area indicated that the electrochemical sensor established in this work can produce a desirable microenvironment with additional electrocatalytic sites.

3.3. Electrochemical detection of TBHQ at Co_3O_4@TAPB-DMTP−COF/GCE

CVs were performed to compare the electrocatalytic oxidation of TBHQ on the bare GCE versus other modified GCEs (Figs. 5, S6). In the

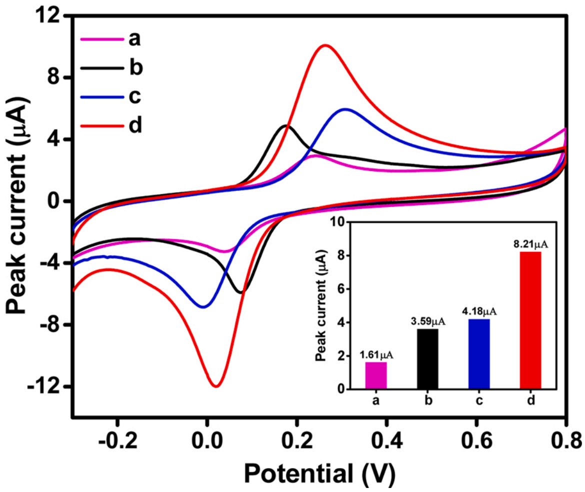

Fig. 5. Cyclic voltammograms obtained for 100 μmol L^{-1} TBHQ at bare GCE (a), Co_3O_4/GCE (b), TAPB-DMTP−COF/GCE (c) and Co_3O_4@TAPB-DMTP−COF/GCE in 0.1 mol · L^{-1} ABS (pH 5.0).

presence of TBHQ, all CV traces showed a new redox peak corresponding to the oxidation and reduction of TBHQ on the electrode surface. As expected, the Co_3O_4@TAPB-DMTP−COF film exhibited the highest catalytic current towards TBHQ. The relative increase in oxidation peak current at Co_3O_4@TAPB-DMTP−COF/GCE was 5.1, 2.3, and 2.0 times higher than bare GCE, Co_3O_4/GCE, and TAPB-DMTP−COF/GCE, respectively. The results indicated that an electrode modified by Co_3O_4@TAPB-DMTP−COF composite can fully harness the virtue of 2 D porous structure from TAPB-DMTP−COF via the electro-activity provided by Co_3O_4.

3.4. *Study of variables that affect the electrocatalytic performance towards TBHQ*

TAPB-DMTP−COF possesses inherent eclipsed stacked structure between two adjacent layers, ideally suited for expediting the charge carrier mobility through multistacked columnar channel. As supported in Fig. 5, the current response at Co_3O_4@TAPB-DMTP−COF/GCE was significantly higher than the Co_3O_4/GCE. Against such backdrop, core-shell-structured Co_3O_4@TAPB-DMTP−COF composite with different masses of Co_3O_4-DMTP (10, 20, 30, 40 mg) were also prepared. With the fixed concentrations of DMTP and TAPB monomer, the TAPB-DMTP−COF shell decreased expectedly as increasing the concentration of Co_3O_4-DMTP (Fig. 6). In particular, when the added mass of Co_3O_4-DMTP was 20 mg, a stable and relative high redox couple was observed, showing the ability of this electrode to construct the most desirable system for the TBHQ detection. The results implied that the appropriate TAPB-DMTP−COF shell is favorable to diffuse TBHQ molecules sufficiently into the electrode surface, leading to a prominent sensing performance.

To investigate the kinetics of electron transfer at Co_3O_4@TAPB-DMTP−COF/GCE, the effect of scan rate on the redox peak currents of TBHQ was recorded by CV (Fig. 7A). Typically, both the anodic (I_{pa}) and cathodic peak current (I_{pc}) of TBHQ gradually increased with the scan rate varying from 25 to 350 mV · s^{-1}. As shown in Fig. 7B, the I_{pa} and I_{pc} of TBHQ at Co_3O_4@TAPB-DMTP−COF/GCE were linearly proportional to the square root of scan rates ($\upsilon^{1/2}$), respectively. These two regression equations are: I_{pa} (μA) = -9.519 + 9.060 $\upsilon^{1/2}$ ($mV^{1/2}$ · $s^{-1/2}$) (R^2 = 0.992); I_{pc} (μA) = 8.206–8.872 $\upsilon^{1/2}$ ($mV^{1/2}$ · $s^{-1/2}$) (R^2 = 0.998), which suggested that the electrochemical reaction on the surface of Co_3O_4@-TAPB-DMTP−COF/GCE is controlled by the diffusion of TBHQ. In addition, as shown in Fig. 6, both the oxidation (E_{pa}) and reduction peak potential (E_{pc}) shifted with the scan rates. The results indicated that the catalytic process of TBHQ at the modified electrode is a quasi-reversible process [31].

The electrochemical oxidation of TBHQ always involved protons transfer and therefore it is expected that the reaction was sensitive to the electrolyte pH. After recording the initial DPV curve of the modified electrode in the blank acetate buffer solutions (ABS), the same electrode was transferred to 0.1 mol · L^{-1} ABS containing 100 μmol L^{-1} TBHQ at selected pH values. As shown in Fig. 7C, the reduction current of TBHQ recorded under pH = 5.0 had a maximum value, indicating the supporting electrolyte at this pH is ideal for TBHQ detection. As seen in Fig. 7D, the reduction peak potential (E_{pc}) shifts linearly and negatively with the pH value, validating the protons have participated in the reduction process. The regression equation is E_{pc} (V) = 0.3206 – 0.053 pH (R^2 = 0.993). According to the Nernst equation [32], $E_{pc} = E^{\theta}$ – (0.059 m/n) pH, the slope of 53 mV pH^{-1} was close to the theoretical value of 0.059 mV · pH^{-1}, indicating an equal number of protons (m) and electrons (n) transferred in the TBHQ reduction process.

In electrochemical detection, an accumulation step was deemed as a simple and efficient method to enhance the determining sensitivity. As

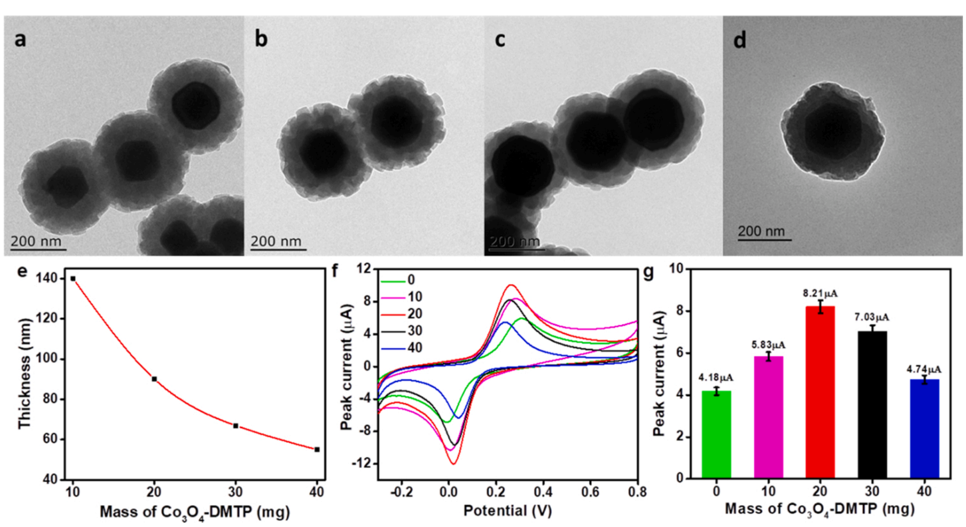

Fig. 6. TEM images of Co_3O_4@TAPB-DMTP−COF composites synthesized with 10 mg (a), 20 mg (b), 30 mg (c) and 40 mg (d) Co_3O_4-DMTP. (e) The average thickness of TAPB-DMTP−COF shell versus the mass of Co_3O_4-DMTP. (f) CVs at Co_3O_4@TAPB-DMTP−COF/GCE in 0.1 mol · L^{-1} ABS (pH 5.0) containing 100 μmol L^{-1} TBHQ with different masses of Co_3O_4-DMTP (0, 10, 20, 30 mg). (g) The oxidation peak current value versus the mass of Co_3O_4-DMTP.

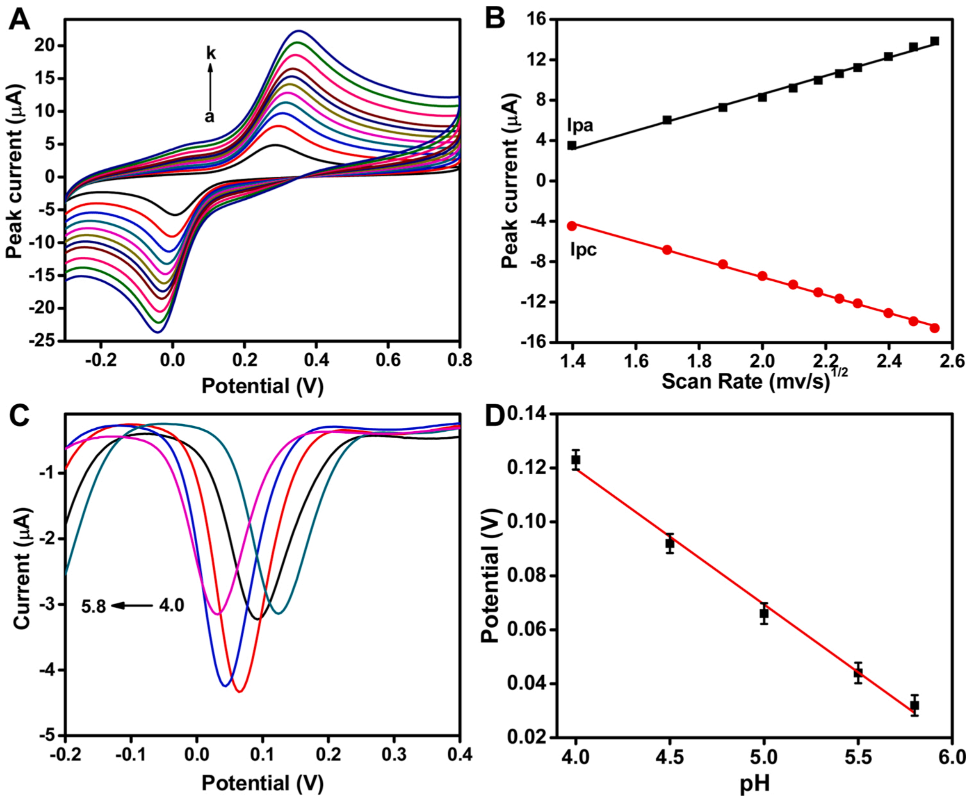

Fig. 7. (A) CVs of 100 μmol L^{-1} TBHQ in 0.1 mol · L^{-1} ABS (pH 5.0) at Co_3O_4@TAPB-DMTP−COF/GCE with various scan rates (from a to k: 25, 50, 75, 100, 125, 150, 175, 200, 250, 300, 350 mV · s^{-1}). (B) Plots of redox peak currents of TBHQ versus the square root of scan rates. (C) DPV curves of 100 μmol L^{-1} TBHQ at Co_3O_4@TAPB-DMTP−COF/GCE in 0.1 mol · L^{-1} ABS with various pH values (4.0, 4.5, 5.0, 5.5, and 5.8). (D) The linear relationship between reduction peak potential and electrolyte pH.

illustrated in Fig. S7, it was found that the accumulation time and accumulation potential can greatly influence the reduction peak current of TBHQ. The effect of accumulation time on the reduction peak current of TBHQ was investigated by varying time from 15 to 90 s (Fig. S7A). The signal intensity increased with the accumulation time increasing up to 60 s. Then it was leveled off with an extending time, which is an indication of the saturated adsorption of TBHQ molecules at the modified electrode. The effect of accumulation potential was further studied with a selected accumulation time of 60 s (Fig. S7B). Particularly, the reduction peak current reached the maximum at 0 V, suggesting the accumulation potential of 0 V is favorable for the TBHQ detection.

3.5. Analytical performance of Co_3O_4@TAPB-DMTP−COF/GCE to TBHQ

The electrocatalytic behavior of the modified electrode at various TBHQ concentrations was investigated by differential pulse voltammetry (DPV) technique. Under the optimal experimental conditions, the catalytic current enhanced gradually with increasing TBHQ concentration in the range of 0.05–400 μmol · L^{-1} (Fig. 8). From the results of Fig. 8B, the reduction peak currents were proportional to TBHQ concentrations over two concentration intervals. The respective two linear regression equations are expressed as follow:

0.05 - 1.00 μmol · L^{-1}: I_{pc} (μA) = 0.0310 C (μmol · L^{-1}) + 0.0218 (R^2 = 0.998)

1.0 - 400 μmol · L^{-1}: I_{pc} (μA) = 0.0170 C (μmol · L^{-1}) + 0.151 (R^2 = 0.997)

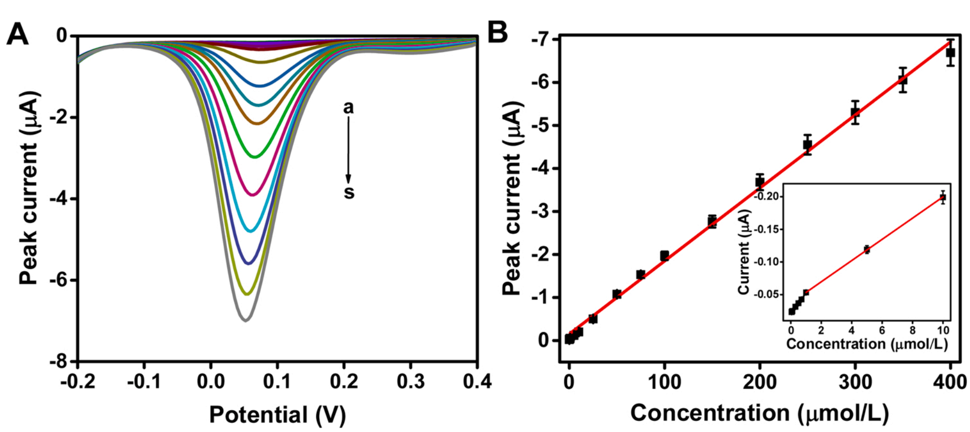

Fig. 8. (A) DPV curves at Co_3O_4@TAPB-DMTP−COF/GCE in 0.1 mol · L^{-1} ABS with different concentrations of TBHQ (from a to s: 0.05, 0.07, 0.1, 0.3, 0.5, 0.7, 1.0, 5.0, 10, 25, 50, 75, 100, 150, 200, 250, 300, 350, 400 μmol · L^{-1}). (B) The calibration curve of the reduction peak current *vs.* TBHQ concentration. Inset: the tendency of current intensity when TBHQ concentrations are low.

The sensitivity at first interval is 0.4388 μA · μM^{-1} · cm^{-2} and the second one is 0.2406 μA · μM^{-1} ·cm^{-2}. Clearly, when the TBHQ concentration is low, the established electrochemical sensor in this work exhibited a higher sensitivity towards TBHQ detection. The two sets of sensitivity values are due to the mass transport limitation and diffusion layer thickness was restricted when the TBHQ concentration increased in the system. Then the decrease of sensitivity at the second analytical linear segment became an inevitable trend [33]. The detection limit (LOD) for TBHQ was estimated to be 0.02 μmol · L^{-1} (S/N = 3). These electrochemical results stated that the Co_3O_4@TAPB-DMTP−COF film on the electrode had excellent activity towards THBQ detection. Furthermore, the analytical performance of Co_3O_4@-TAPB-DMTP−COF/GCE to TBHQ was compared with other electrode materials. From Table 1 [5,9,34–37], it can be observed that the fabricated sensor exhibited dominance in wider linear range, and lower LOD, which is comparable with other reported sensing materials. Such excellent analytical performance could be attributed to its unique structure and composition of Co_3O_4@TAPB-DMTP−COF composite. The Co_3O_4 itself is an excellent electrocatalyst. The abundant Co^{3+} catalytic sites in Co_3O_4 are favorable to catalyze TBHQ. By engineering TAPB-DMTP−COF with Co_3O_4, the larger surface area and porous structure will enhance the electrocatalytic activity towards TBHQ. Besides, TAPB-DMTP−COF is constructed from two organic linkers via Schiff base reaction. The aromatic ring of TBHQ can highly interact with TAPB-DMTP−COF via π-π stacking, facilitating the adsorption of TBHQ on the electrode surface.

3.6. Stability and reproducibility of Co_3O_4@TAPB-DMTP−COF electrode

To evaluate the repeatability of Co_3O_4@TAPB-DMTP−COF electrode, one modified electrode was applied for the detection of 50 μmol L^{-1} TBHQ in 0.1 mol · L^{-1} ABS (pH 5.0). After ten successive DPV scans, the calculated relative standard value (R.S.D.) was 2.7 %. In the above system, DPV currents on six electrodes fabricated from different batches were recorded to investigate the reproducibility of the fabricated sensor. The R.S.D. was calculated as 3.4 %. The above results demonstrated that the Co_3O_4@TAPB-DMTP−COF modified electrode has acceptable repeatability and reproducibility.

Stability is another important characteristic for the practical detection of TBHQ. It was found that there is no significant decrease in current responses even after eighty successive detection of 50 μmol L^{-1} TBHQ. Furthermore, the long-time stability of the Co_3O_4@TAPB-DMTP−COF/GCE was also investigated. The DPV curve was recorded with a time interval of 24 h. Approximately, the electrocatalytic performance at the as-prepared sensor remained 96.5 % of its initial current signal after four weeks storage at ambient temperature. These findings revealed the operational and long-time stability of the Co_3O_4@TAPB-DMTP−COF/GCE. The outstanding stability is due to the existence of TAPB-DMTP−COF shell in the Co_3O_4@TAPB-DMTP−COF composite, which efficiently protected the electrocatalytic performance towards TBHQ detection. Compared with other electrode materials, TAPB-DMTP−COF has a better electrochemical stability owing to its strong covalent interactions, which grant a longer cycle life in electrochemical tests.

Table 1
Comparison of Co_3O_4@TAPB-DMTP−COF/GCE-based electrochemical sensor with other reported sensors for the detection of TBHQ.

Electrode	Linear range (μmol · L^{-1})	Detection limit (μmol · L^{-1})	Reference
Peroxidase/Naf/SEP/CNT/CPE	9.9−59.1	2.47	[5]
PVP-CTAB/Au-PVP-Gr/GCE	0.02−100	0.009	[9]
MIP/AuNPs/EGP	0.08−100	0.07	[34]
MnO_2/ERGO/GCE	1−300	0.8	[35]
PEDOT:PSS/DMSO	0.5−200	0.15	[36]
PdAuNPs/ERGO/GCE	3−360	0.28	[37]
Co_3O_4@TAPB-DMTP-COF/GCE	0.05−1 1−400	0.002	This work

3.7. Influence of co-existing ions and analysis application

Phenolic antioxidants, including butylated hydroxyanisole (BHA), butylated hydrotoluene (BHT), and benzoic acid, have similar structure with TBHQ, and they are usually in mixtures with food samples. Thus it is necessary to study the interference of these phenolic antioxidants on the current response of TBHQ. Fig. S8A-C shows the respective CV responses of 5 μmol L^{-1} TBHQ in the presence and absence of BHA, BHT, and benzoic acid. It was found that 12-fold excess of benzoic acid, and 10-fold excess of BHA, BHT has negilible effect on the TBHQ determination. The tolerant limit for the foreign species was defined on the basis of signal change within ± 5% with respect to only TBHQ solution. In addition, vitamin E is also a common antioxidant that is relatively abundant in food oils. As shown in Fig. S8D, the addition of 20-fold excess of vitamin E does not affect both the anodic and cathodic peaks of TBHQ.

In commercial edible oil samples, some other impurities, such as ascorbic acid, phenolic compounds (propyl gallate, hydroxyphenol, and hydroquinone), glycerine, and ions can possibly interfer the TBHQ determination. Therefore, the effect of these interferences were also conducted with the Co_3O_4@TAPB-DMTP−COF sensor using CV technique at the optimized condition (Table 2). From the tabulation of Table 2, it was found that the Co_3O_4@TAPB-DMTP−COF sensor exhibits an excellent selectivity towards TBHQ. All these results suggested that the constructed TBHQ sensor in this work has a great promise for TBHQ determination in edible oil samples.

Edible oil is the necessity in our daily life. Only keeping them in a safety level can ensure our body's health. The allowable level of TBHQ in edible oil samples has been formulated as 200 μg · g^{-1} in the "National Standard GB2760−96 Sanitary of Using Food Additives".In this work, DPV method was utilized to estimate the feasibility of the Co_3O_4@TAPB-DMTP−COF/GCE sensor and the analysis of TBHQ in edible oil samples was implemented by standard addition. Commercial peanut oil, soybean oil and colza oil were extracted as stated in the experimental section. Under the optimized condition, a 50 μL aliquot of the extract was added to 10 mL 0.1 mol · L^{-1} ABS in the electrochemical cell. Then, the above electrochemical cell was spiked with TBHQ at three levels (0, 2 and 5 μmol · L^{-1}). For each concentration, six repetitive measurements were conducted by DPV method. As displayed in Table 3, the recoveries were found in the range of 97.0–104.2 %, which indicates that the proposed electrochemical sensor is reliable and feasible for TBHQ detection in real samples. The accuracy of the method was further validated by traditional HPLC using variance ratio F-test and Student's *t*-test (Table 3). The chromatographic conditions for analyzing TBHQ in edible oil samples were set according to the national standard method of China (GB/T 21512−2008). A 50 μL aliquot was injected into the HPLC equipment. The chromatographic parameters for TBHQ detection are shown below: flow rate: 0.8 mL · min^{-1}; column temperature: 30 °C; UV/vis detector wavelength: 280 nm; organic phase solution: methanol-acetonitrile (1:1); aqueous phase: 1.8 % acetic acid. As exhibited in Table 3, it can be seen that the calculated values of F-test and *t*-test were

Table 2
The tolerance limit of interferences in the 5 μmol · L^{-1} TBHQ.

Interference	Tolerance limit	Interference	Tolerance limit
Fe^{3+}, Mg^{2+}, Cu^{2+}, Mn^{2+}, Ca^{2+}, Zn^{2+}, K^+, Na^+, PO_4^{3-}, SO_4^{2-}, Cl–, NO_3–	500	vitamin E, ascorbic acid	20
		benzoic acid	12
propyl gallate	50	BHA, BHT	10
hydroxyphenol, hydroquinone	30	glycerine	5

Table 3
Detection of TBHQ in edible oil samples.

Samples	Added (μmol ·L^{-1})	Found by DPV[a] (μmol · L^{-1})	Recovery (%)	Found by HPLC[a] (μmol · L^{-1})	Calculated F-value[b]	Calculated t-value[c]
	0.00	0.52 ± 0.08	–	0.46 ± 0.14	3.06	0.91
Peanut oil	2.00	2.57 ± 0.26	102.6	2.55 ± 0.34	1.71	1.61
	5.00	5.61 ± 0.42	101.8	5.78 ± 0.27	2.42	0.83
	0.00	0.33 ± 0.10	–	0.43 ± 0.13	1.69	0.33
Soybean oil	2.00	2.27 ± 0.52	97.0	2.45 ± 0.29	3.21	0.74
	5.00	5.34 ± 0.12	100.2	5.39 ± 0.06	4.00	0.91
	0.00	0.21 ± 0.02	–	0.24 ± 0.03	2.25	2.04
Colza oil	2.00	2.23 ± 0.12	101.0	2.25 ± 0.07	2.94	0.35
	5.00	5.42 ± 0.28	104.2	5.17 ± 0.15	3.48	1.93

[a] The average of six determinations (± S.D.).
[b] The theoretical values of F-value at the confidence level of 90 % is $F_{5,\ 5} = 5.05$.
[c] The theoretical values of t-value at the confidence level of 95 % is $t_{0.05,\ 10} = 2.23$.

below the theoretical values, suggesting there is no significant difference in these two analytical methods. Compared with the reference method, the proposed electrochemical sensor in our work can meet the demands of developing a rapid, cost-effective, and accurate detection of TBHQ in real samples.

4. Conclusion

A novel core-shell-structured composite composed of Co_3O_4 conformally coated with TAPB-DMTP−COF has successfully constructed through monomer-mediated in situ growth strategy. The Co_3O_4 core acts as the electrocatalytic active centers and the multistacked columnar channels provided by 2 D TAPB-DMTP−COF shell can largely expedite charge carrier mobility to the Co^{3+} active sites. Furthermore, the outer TAPB-DMTP−COF shell plays a critical role in improving electrochemical stability, ensuring a longer lifespan of the Co_3O_4@TAPB-DMTP−COF/GCE sensor. Taking these advantages together, the Co_3O_4@TAPB-DMTP−COF composite is capable to sense TBHQ molecules with enhanced electrochemical sensing performances. Compared with traditional HPLC measurements, the comparable accuracy of this established sensor should have more implications in detecting TBHQ from complicated real samples. Given the predetermined and elegant combined properties of core-shell-structured composites, we envision that engineering electrocatalytic components to COF is certainly possible to stimulate the development of COF in electrochemical applications.

CRediT authorship contribution statement

Yuling Chen: Conceptualization, Data curation, Methodology, Project administration, Writing - original draft. **Yao Xie:** Formal analysis, Investigation, Software, Validation. **Xin Sun:** Data curation, Investigation, Validation. **Yang Wang:** Funding acquisition, Project administration, Resources, Supervision, Writing - review & editing. **Yi Wang:** Data curation, Resources, Validation, Writing - review & editing.

Declaration of Competing Interest

The authors declare that they have no known competing financial interests or personal relationships that could have appreared to influence the work reported in this paper.

Acknowledgements

This work was supported by the National Natural Science Foundation of China (21205103), Jiangsu Provincial Nature Foundation of China (BK2012258), Top-notch Academic Programs Project of Jiangsu Higher Education Institutions (TAPP), and a project funded by the Priority Academic Program Development of Jiangsu Higher Education Institutions (PAPD).

Appendix A. Supplementary data

Supplementary material related to this article can be found, in the online version, at doi:https://doi.org/10.1016/j.snb.2021.129438.

References

[1] K.Z. Sanidad, E. Sukamtoh, W.C. Wang, Z.Y. Du, E. Florio, L.L. He, H. Xiao, E. A. Decker, G.D. Zhang, Oxidative conversion mediates antiproliferative effects of tert-butylhydroquinone: structure and activity relationship study, J. Agric. Food Chem. 64 (2016) 3743–3748.
[2] E.S. Almeida, F.M. Portela, R.M.F. Sousa, D. Daniel, G.H. Terrones, E.M. Richter, R. A.A. Muñoz, Behaviour of the antioxidant tert-butylhydroquinone on the storage stability and corrosive character of biodiesel, Fuel 90 (2011) 3480–3484.
[3] G.J. Van Esch, Toxicology of tert-butylhydroquinone (TBHQ), Food Chem. Toxicol. 24 (1986) 1063–1065.
[4] S. Kashanian, J.E.N. Dolatabadi, DNA binding studies of 2-tert-butylhydroquinone (TBHQ) food additive, Food Chem. 116 (2009) 743–747.
[5] T.R.D. Oliveira, G.F. Grawe, S.K. Moccelini, A.J. Terezo, M. Castilho, Enzymatic biosensors based on ingá-cipó peroxidase immobilised on sepiolite for TBHQ quantification, Analyst 139 (2014) 2214–2220.
[6] X.Q. Li, C. Ji, Y.Y. Sun, M.L. Yang, X.G. Chu, Analysis of synthetic antioxidants and preservatives in edible vegetable oil by HPLC/TOF-MS, Food Chem. 113 (2009), 692-670.
[7] J. Li, Y.L. Bi, S.D. Sun, D. Peng, Simultaneous analysis of tert-butylhydroquinone, tert-butylquinone, butylated hydroxytoluene, 2-tert-butyl-4-hydroxyanisole, 3-tert-butyl-4-hydroxyanisole, α-ocopherol, γ-tocopherol, and δ-tocopherol in edible oils by normal-phase high performance liquid chromatography, Food Chem. 234 (2017) 205–211.
[8] L. Wang, R. Yang, J.J. Li, L.B. Qu, A selective and sensitive tert-butylhydroquinone sensor based on synergy of CTAB and AuNPs-PVP-graphene nanohybrids, Ionics 22 (2016) 415–423.
[9] A.P. Côté, A.I. Benin, N.W. Ockwig, M. O'Keeffe, A.J. Matzger, O.M. Yaghi, Porous, crystalline, covalent organic frameworks, Science 310 (2005) 1166–1170.
[10] Y. Yuan, Y.J. Yang, G.S. Zhu, Multifunctional porous aromatic frameworks: state of the art and opportunities, Energy Fuels 1 (2020), 100037.
[11] L.J. Zhu, Y.B. Zhang, Crystallization of covalent organic frameworks for gas storage applications, Molecules 22 (2017) 1149.
[12] Z.F. Wang, S.N. Zhang, Y. Chen, Z.J. Zhang, S.Q. Ma, Covalent organic frameworks for separation applications, Chem. Soc. Rev. 49 (2020) 708–735.
[13] Y. Yusran, H. Li, X.Y. Guan, Q.R. Fang, S.L. Qiu, Covalent organic frameworks for catalysis, Energy Fuels 1 (2020), 100035.
[14] M.X. Wu, Y.W. Yang, Applications of covalent organic frameworks (COFs): from gas storage and separation to drug delivery, Chin. Chem. Lett. 28 (2017) 1135–1143.
[15] X.G. Liu, D.L. Huang, C. Lai, G.M. Zeng, L. Qin, H. Wang, H. Yi, B.S. Li, S.Y. Liu, M. M. Zhang, R. Deng, Y.K. Fu, L. Li, W.J. Xue, S. Chen, Recent advances in covalent organic frameworks (COFs) as a smart sensing material, Chem. Soc. Rev. 48 (2019) 5266–5302.
[16] L.Y. Wang, B. Dong, R.L. Ge, F.X. Jiang, J.K. Xu, Fluorene-based two-dimensional covalent organic framework with thermoelectric properties through doping, ACS Appl. Mater. Interfaces 9 (2017) 7108–7114.
[17] S. Bhunia, S.K. Das, R. Jana, S.C. Peter, S. Bhattacharya, M. Addicoat, A. Bhaumik, A. Pradhan, Electrochemical stimuli-driven facile metal-free hydrogen evolution from pyrene-porphyrin-based crystalline covalent organic framework, ACS Appl. Mater. Interfaces 9 (2017) 23843–23851.
[18] H. Xu, J. Gao, L. Jiang, Stable, crystalline, porous, covalent organic frameworks as a platform for chiral organocatalysts, Nat. Chem. 7 (2015) 905–912.
[19] S.N. Liu, C.L. Hu, Y. Liu, X.Y. Zhao, M.L. Pang, J. Lin, One-pot synthesis of DOX@ covalent organic framework with enhanced chemotherapeutic efficacy, Chem. Eur. J. 25 (2019) 4315–4319.
[20] X.H. Ma, C.H. Pang, S.H. Li, Y.H. Xiong, J.P. Li, J.H. Luo, Y. Yang, Synthesis of Zr-coordinated amide porphyrin-based two-dimensional covalent organic framework

at liquid-liquidinterface for electrochemical sensing of tetracycline, Biosens. Bioelectron. 146 (2019), 111734.
[21] R.G. Chaudhuri, S. Paria, Core/shell nanoparticles: classes, properties, synthesis mechanisms, characterization, and applications, Chem. Rev. 112 (2012) 2373–2433.
[22] M.B. Gawande, A. Goswami, T. Asefa, H.Z. Guo, A.V. Biradar, D.L. Peng, R. Zboril, R.S. Varma, Core-shell nanoparticles: synthesis and applications in catalysis and electrocatalysis, Chem. Soc. Rev. 44 (2015) 7540–7590.
[23] H.X. Dai, Y.L. Chen, X.Y. Niu, C.J. Pan, H.L. Chen, X.G. Chen, High-performance electrochemical biosensor for nonenzymatic H_2O_2 sensing based on Au@C-Co_3O_4 heterostructures, Biosens. Bioelectron. 118 (2018) 36–43.
[24] Z.T. Zhao, J. Zhang, W.D. Wang, Y.J. Sun, P.W. Li, J. Hu, L. Chen, W.P. Gong, Synthesis and electrochemical properties of Co_3O_4-rGO/CNTs composites towards highly sensitive nitrite detection, Appl. Surf. Sci. 485 (2019) 274–282.
[25] Y. Pan, H.J. Ren, H.W. Du, F.Y. Cao, Y.F. Jiang, H.J. Du, D.W. Chu, Active site engineering by surface sulfurization for a highly efficient oxygen evolution reaction: a case study of Co_3O_4 electrocatalysts, J. Mater. Chem. A 6 (2015) 22497–22502.
[26] J. Sun, G.L. Yu, L.L. Liu, Z.F. Li, Q.B. Kan, Q.S. Huo, J.Q. Guan, Core-shell structured Fe_3O_4@SiO_2 supported cobalt(II) or copper(II) acetylacetonate complexes: magnetically recoverable nanocatalysts for aerobic epoxidation of styrene, Catal. Sci. Technol. 4 (2014) 1246–1252.
[27] B.J. Smith, A.C. Overholts, N. Hwang, W.R. Dichtel, Insight into the crystallization of amorphous imine-linked polymer networks to 2D covalent organic frameworks, Chem. Commun. 52 (2016) 3690–3693.
[28] S.Y. Liu, L. Teng, Y.M. Zhao, Z. Liu, J.W. Zhang, M. Ikram, A.U. Rehman, L. Li, K. Y. Shi, Facile route to synthesize porous hierarchical Co_3O_4/CuO nanosheets with high porosity and excellent NO_x sensing properties at room temperature, Appl. Surf. Sci. 450 (2018) 91–101.
[29] S. Biswas, H. Naskar, S. Pradhan, Y. Wang, R. Bandyopadhyay, P. Pramanik, Simultaneous voltammetric determination of adrenaline and tyrosine in real samples by neodymium oxide nanoparticles grafted graphene, Talanta 206 (2020), 120176.
[30] Y. Ma, Y.C. Wang, D.H. Xie, Y. Gu, H.M. Zhang, G.Z. Wang, Y.X. Zhang, H.J. Zhao, P.K. Wong, NiFe-layered double hydroxide nanosheet arrays supported on carbon cloth for highly sensitive detection of nitrite, ACS Appl. Mater. Interfaces 10 (2018) 6541–6551.
[31] D.M. Song, J.F. Xia, F.F. Zhang, S. Bi, W.J. Xiang, Z.H. Wang, L. Xia, Y.Z. Xia, Y. H. Li, L.H. Xia, Multiwall carbon nanotubes-poly(diallyldimethylammonium chloride)-graphene hybrid composite film for simultaneous determination of catechol and hydroquinone, Sensor. Actuat. B: Chem. 206 (2015) 111–118.
[32] J.J. Zhang, S.Q. Cui, Y.P. Ding, X.X. Yang, K. Guo, J.T. Zhao, Ordered mesoporous Co_3O_4 nanospheres/reduced graphene oxide composites for rutin detection, Ceram. Int. 44 (2018) 7858–7866.
[33] Y. Wang, L. Wang, H.H. Chen, X.Y. Hu, S.Q. Ma, Fabrication of highly sensitive and stable hydroxylamine electrochemical sensor based on gold nanoparticles and metal-metalloporphyrin framework modified electrode, ACS Appl. Mater. Interfaces 8 (2016) 18173–18181.
[34] L.M. Fan, Q.Q. Hao, X.W. Kan, Three-dimensional graphite paper based imprinted electrochemical sensor for tertiary butylhydroquinone selective recognition and sensitive detection, Sensor. Actuat. B: Chem. 256 (2018) 520–527.
[35] W. Cao, Y. Wang, Q.F. Zhuang, L.Y. Wang, Y.N. Ni, Developing an electrochemical sensor for the detection of tert-butylhydroquinone, Sensor. Actuat. B: Chem. 293 (2019) 321–328.
[36] Q.Y. Tian, J.K. Xu, Q. Xu, X.M. Duan, F.X. Jiang, L.M. Lu, H.Y. Jia, Y.H. Jia, Y.Y. Li, Y.F. Yu, A Poly(3,4-ethylenedioxythiophene):poly(styrenesulfonate) -based electrochemical sensor for tert-butylhydroquinone, Microchim. Acta 186 (2019) 772.
[37] X.Y. Yue, X.Y. Luo, Z.J. Zhou, Y.H. Bai, Selective electrochemical determination of tertiary butylhydroquinone in edible oils based on an in-situ assembly molecularly imprinted polymer sensor, Food Chem. 289 (2019) 84–94.

YuLing Chen received her bachelor's degree in applied chemistry from Changshu Institute of Technology in 2017. She received her M. Sc. degree in Chemistry from Yangzhou University in 2020. She is now pursuing her Ph.D. degree in Soochow University. Her work is is conducting research on the synthesis of COF@polymer core-shell composite and its application for metal ions detection.

Yao Xie received her bachelor's degree in applied chemistry from Shanghai University in 2018. She is now pursuing her M. Sc. degree in Yangzhou University. Her work is focused on the design and preparation of covalent organic framework composite with excellent enzymatic properties for electrochemical biosensor.

Xin Sun received her bachelor's degree in applied chemistry from Yangzhou University in 2019. She is now pursuing her M. Sc. degree in Yangzhou University. Her work is focused on the design and preparation of bimetallic covalent organic frameworks materials for electrochemical biosensor.

Yang Wang is a professor in analytical chemistry at the School of Chemistry and Chemical Engineering, Yangzhou University. He received his Ph.D. degree in analytical chemistry from Northeastern University in 2007. His current interests focus on synthesis and application of metal-organic framework and covalent organic framework as novel electrode materials for molecular recognition and sensing.

Yi Wang is currently a professor at Wenzhou Medical University, and Wenzhou Institute, University of Chinese Academy of Sciences. He obtained his PhD in 2010 from Max-Planck Institute for Polymer Research in Mainz, Germany. After that he worked as a research fellow at Austrian Institute of Technology, Austria and Nanyang Technological University, Singapore from 2011 to 2015. He has published over 50 peer-reviewed journal papers on nanomaterials based biosensors. His research interests include the development of plasmonic nanostructure, nanocomposites, metal-organic framework and peptide-functionalized materials for optical and electrochemical biosensors.